Response surface approach to minimize the residual stresses in full penetration pulsed TIG weldments of Ti-5Al-2.5Sn alloy

M. Junaid [a,*], FN.Khan[b], MN Baig[c,*], J.Haider[d],

[a]Faculty of Mechanical Engineering, Ghulam Ishaq Khan Institute of Engineering Science and Technology, Topi 23640, Pakistan

[b]Faculty of Materials and Chemical Engineering, Department of Material Science,Ghulam Ishaq Khan Institute of Engineering Science and Technology, Topi 23640, Pakistan

[c] Pakistan welding institute, PO box 1781 Islamabad, Pakistan

[d] School of Engineering, Manchester Metropolitan University, Manchester, M1 5GD, UK

*** Corresponding author, Phone +92 336 9151127**

massab@giki.edu.pk **(Massab Junaid)**

Abbreviations

P-TIG	pulsed TIG
FZ	fusion zone
BM	base material
HAZ	heat affected zone
DOE	design of experiments
BBD	Box-Bhenkhen design
CCD	central composite design

Abstract

Pulsation of current in TIG welding is employed to obtain good quality weldments. Peak current, background current and welding speed in TIG welding are important parameters and their effects on the induced residual stresses are studied using Box-Bhenkhen Design methodology. The location of maximum residual stress was found to be close to the weld centerline. Longitudinal and transverse residual stresses at this location were found to be dependent on the pulsed TIG (P-TIG) welding input parameters. However, using DOE approach, welding speed was found to have the most dominant influence on the stress values. In order to minimize the residual stresses, a reduction in heat input also led to reduction of weld pool penetration. The results of multi-response optimization showed that in order to achieve a full penetration weldment, a minimum value of 235 MPa for longitudinal and 84 MPa for transverse residual stress will be attained. A weldment with these features can be obtained by using a high value of peak current and a high value of welding speed.

Introduction

Response surface methodology (RSM) is a design of experiment (DOE) technique which is mostly used nowadays for effectively optimizing the input parameters in the manufacturing process of interest. ~~process of interest~~ [1–3]. Using this approach, the

functional relationship between the response and several input variables can be established and the ~~controllable~~ controlling factors having dominant influence on the response can be distinguished. Furthermore, all the effects of the considered factors and interactions can be determined, unlike Taguchi and factorial designs using RSM [4]. In RSM, central composite design (CCD) and Box-Behnken design (BBD) are the most widely used techniques for developing second order models. CCD, is a fractional factorial design which normally has 5 levels for each factor and has been used in number of studies for investigation of welding process [3,5]. In the present work, BBD was chosen for the experimental investigation of P-TIG welding process due to the following reasons:

1. Unlike CCD, for BBD the study region and operative region are the same due to which each input factor is investigated over its full range.
2. In CCD the design matrix also have some star points which lie outside the range of input factors and corner points which occur at the extreme values of the input factors.
3. Since BBD is a three level design (three values for each of the input parameters), it is able to investigate the P-TIG welding process with few number of runs as compared to CCD [3,4].
4. For the case of welding, defects such as lack of penetration, undercut, excessive melting and expulsion may result by performing experiments at these corner and star points. For this reason BBD is usually chosen since it avoids the corner and start points and the design matrix is around the center point of the working range [6].

Studies focusing on the application of DOE methods to investigate the effect of TIG welding parameters on the performance of titanium alloys were also reviewed in detail. Peak current, base current, pulse frequency and pulse-on-time were identified as the four variables which define the pulsed current in P-TIG welding process. Most of the studies targeted the optimization of pulsed current by finding the ~~best possible combination of~~ optimum peak value, base value, pulse frequency and pulse-on-time.

Balasubramanian et al. (2007) used the RSM approach to find the dependence of FZ grain~~s~~ size and its microhardness on the pulsed current variable (peak current, base current, pulse frequency and pulse-on-time) for 1.6 mm thick Ti-6Al-4V alloy sheet [7]. They reported a significant influence of the pulsed current variables on the FZ grains size and its microhardness and performed a multi-response optimization to minimize the FZ grain size and maximize its microhardness. In another work, they studied the effect of ~~pulsed~~ pulse current variables on the weld pool geometry (front height, front width, back height, back width) in P-TIG welding of 1.6 mm thick Ti-6Al-4V alloy sheet [8]. They further performed the multi objective optimization using lexicographic method in which a level of preference is set for each of the target objective (minimize back height, front height and front width). Balasubramanian et al. (2008) worked on the effect of pulsed current variables on the impact toughness of P-TIG welded Ti-6Al-4V alloy sheet by using GEP Box which is another DOE approach [9]. They reported that peak current and pulse frequency have major influence on the FZ grain size and impact toughness and also observed an inverse relationship between FZ grain size and impact toughness. In another study, they developed a mathematical model to relate the tensile properties of the Ti-6Al-4V weldments with the pulsed current variables in pulsed TIG welding. They employed central composite method which is a type of RSM and reported a significant influence of ~~pulsed~~ pulse current on the tensile properties [10].

The opportunities available to optimize the pulsed TIG welding process for titanium alloys, especially Ti-5Al-2.5Sn alloy using DOE approach, have not been explored to its full potential. Some studies are available which aimed at improvingthe weld pool shape, FZ grain size and tensile properties of titanium alloys weldments by optimizing the pulsed current parameters (peak current, base current, pulse frequency and pulse-on-time) only. The following points are very important and must be considered for further improvement of the pulsed TIG welding process.

a. Residual stresses play a significant role in the operational life of welded structures. The emerging welding techniques such as pulsed laser and electron beam welding have an advantage of heat sources power density significantly greater than TIG welding. Consequently, to achieve full

penetration in welding, much less overall heat input is required in LBW and EBW leading to lower level of induced residual stresses [11–13].

b. To further improve the pulsed TIG welding process for titanium alloys, the optimization process should also include the minimization of residual stresses.
c. The work of Olabi et al. (2007) showed that in pulsed LBW process, the welding speed was found to be the input factor having the most significant influence on the residual stresses in the weldments [14]. Hence, for pulsed TIG welding process, the input factor of welding speed must be considered as the input factor and included in addition to pulsed current.

This work aims to employ the Box-Bhenkhen design methodology to developa relationship between the P-TIG welding input parameters of peak current, background current and welding speed and the responses of weld pool penetration, longitudinal and transverse residual stresses. The input parameters having a dominant influence on the output responses are identified and criteria are established to effectively minimize the residual stresses in the weldments.

Methodology

Material and Methods

P-TIG welding was performed on Ti-5Al-2.5Sn alloy sheet with a thickness of 1.6 mm,provided by Continental Steel and Tube Company USA. Coupons each of size 75 mm × 100 mm were welded in butt configuration such that a final size of 150mm × 100 mm was obtained. The sheet was clamped during the welding operation to avoid any possible gap due to sheet movement during to the welding process. To protect the molten titanium pool from oxidation, the flow of argon with a flow rate in the range 10 to12 L/min was maintained during and after the welding operation. The details of residual stress measurement procedure and microscopy are given in detail in the author's previous work[15].

Experimental work

A review of literature suggests that the peak current, background current and welding speed are the three critical factors in P-TIG welding process [16–19]. The upper and lower limits of the critical factors are identified based on initial experimentation. This required a large number of trial runs during which the all other input parameters were fixed while the factor of interest was varied such that the resultant properties of the welds are acceptable. Trial samples in bead on plate (BoP) configuration were prepared to determine the working range for each of the input parameters. Based on this criterion, the following observations were made:

a. A lack of penetration and melting of the weld pool was observed if the peak current is less than 24 A. Moreover, too un-even shape of the weld pool (ripples) appeared at the back side of the sample and overheating of the tungsten electrode was observed, if the welding current was more than 36 A.
b. The welding arc was unstable if the background current was less than 12 A, and led to incomplete penetration in the sample. Moreover, arc wandering took place if the background current increased beyond 18 A, resulting in a very large weld pool width. Weld pool became shallow at the top and a rise in bead height was observed at the back side.
c. The selection of suitable range for the welding speed depends on the pulse overlap. Increasing the speed beyond 36 mm/min resulted in a very small pulse overlap due to which the weld bead was not smooth and continuous fusion was not obtained throughout the bead length. Similarly, a welding speed less than 24 mm/min resulted in a significant rise in bead height and excessive width of weld pool on both sides of the sample was observed.

After a number of experiments, the range of important input parameters were found as presented in Table 1. The remaining welding parameters were held fixed at the values as shown in Table 2.

Table 1. Range of TIG welding input parameters

Input factors	Units	Lower value	Upper value
Welding speed	mm/min	24	36
Peak current	A	24	36
Background current	A	12	18

Table 2. Values of TIG welding input parameters which are kept constant

Pulse Width (ms)		Pre-Purge	Post Purge (sec)	Voltage (V)	Arc Gap (mm)	Tungsten Electrode	Electrode Dia (mm)
High	Low						
8	4	10	10	10	2 mm	2 % Th	1.6

~~Developing the model~~ ***Model development***

The experimental design matrix was developed using the Box-Behnken design (BBD) approach. This is a type of response surface methodology (RSM) which utilizes a mathematical and statistical approach for developing appropriate models for the predicting the responses of interest. In order to optimize a specific response, first a functional relationship between the input factors and the response is established. For implementation of BBD, three levels of each input factors were chosen and the relationship between a specific output response and the input factors is as shown in Eq. (1)

$$y = b_o + \sum b_i X_i + \sum b_{ii} X_{ii}^2 + \sum b_{ij} X_i X_j + e \quad (1)$$

”y” represents a specific output response and “X_i” represents the input factors. The first summation term in Eq. (1) represents the effects of all the main input factors, whereas the second and third summation term represents the quadratic effects and two factor interactions respectively. The coefficient “b” represents the weights of the input factors and an extensive regression analysis was performed to calculate the values of these

coefficients in the functional relationship. Since the problem is a multiple-input-multiple-output system, the regression analysis is very extensive and is solved using a computer based algorithm. In the present study, Design expert V10 was used to perform the regression analysis for the measured responses based on RSM. A fit summary suggests an appropriate model for the start. Different models such as “mean”, “linear”, “2FI”, and “quadratic” can be used in the BBD analysis. It should be noted that “cubic” and higher order models are aliased (solution does not converges) for BBD and should not be used [20]. Statistical analysis of sequential F test, lack of fit tests etc. were then performed to assess the validity of the developed models. The following sequence of statistical tests were adopted to converge to the most suitable regression model.

Table 3 presents the experimental design matrix in terms of the coded and actual factors. Standard order shows the standard presentation sequence of the BBD experiment combination whereas the experiments are actually conducted according to the run order. It is to be noted that the run order is different than the standard order of the experimental design and the run order is followed while performing the experiments.

Table 3. Experimental design matrix for BBD in terms of coded and actual factors

Std. Ord	Run. Ord	Coded Factors			Actual Factors		
		Peak current (A)	Background current (B)	Speed (C)	Peak current (P)	Background current (R)	Speed (S)
Units					A	A	mm/min
1	13	-1	-1	0	24	12	30
2	7	1	-1	0	36	12	30
3	11	-1	1	0	24	18	30
4	8	1	1	0	36	18	30
5	1	-1	0	-1	24	15	24
6	12	1	0	-1	36	15	24
7	6	-1	0	1	24	15	36
8	10	1	0	1	36	15	36
9	3	0	-1	-1	30	12	24
10	9	0	1	-1	30	18	24
11	5	0	-1	1	30	12	36
12	2	0	1	1	30	18	36
13	4	0	0	0	30	15	30
14	15	0	0	0	30	15	30
15	14	0	0	0	30	15	30

Results and Discussions

Based on the scheme of parametric investigation established related to design of experiments, tests were performed to record the output responses. The run order listed in Table 3was followed and the measured responses are presented in **Table 4**.

Table 4. Measured values of the responses.

Std.order	Run.order	Input factors			Output responses		
		Peak current (P)	Back current (R)	Speed (S)	Penetration Full=1/Partial=0	Longitudinal residual stress (RS_L)	Transverse residual stresses (RS_T)
		A	A	mm/min	1 or 0	MPa	MPa
1	13	24	12	30	0	211	81
2	7	36	12	30	0	214	78
3	11	24	18	30	1	245	148
4	8	36	18	30	1	261	97
5	1	24	15	24	0	277	105
6	12	36	15	24	0	274	126
7	6	24	15	36	0	196	62
8	10	36	15	36	1	196	72
9	3	30	12	24	0	222	93
10	9	30	18	24	1	285	154
11	5	30	12	36	0	175	53
12	2	30	18	36	1	234	84
13	4	30	15	30	0	221	101
14	15	30	15	30	0	238	93
15	14	30	15	30	0	229	82

Weld pool penetration

The top and bottom sides for some of the welded samples of DOE specimens are shown in Figure 1. The images correspond to the welding parameters given by the Std. order of **Table 4**. In Figure 1, it can be seen that the weld bead has a significant bottom width for some of the welding conditions (e.g. No. 2, No. 11) and therefore can be

considered as full penetration weldments. The molten pool may not appear at the bottom side of the welded plate for other welding conditions (e.g.: No. 6) and therefore has a partial penetration. Hence the bottom width of the weld pool may be negligible for some of the welding conditions. Among all the 15 weldments in**Table 4**, the weld pool in the sampleNos. 2, 3, 11, 14 and 15 extend up to the bottom side of the sample (full penetration) and vice versa for other welding conditions.

(a)

Top View

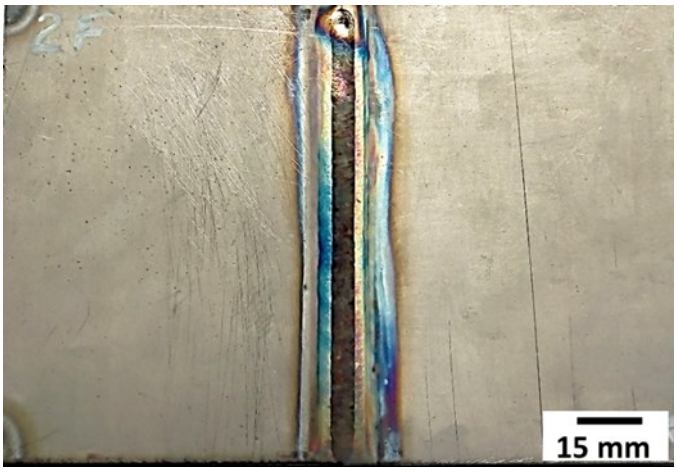

Bottom View

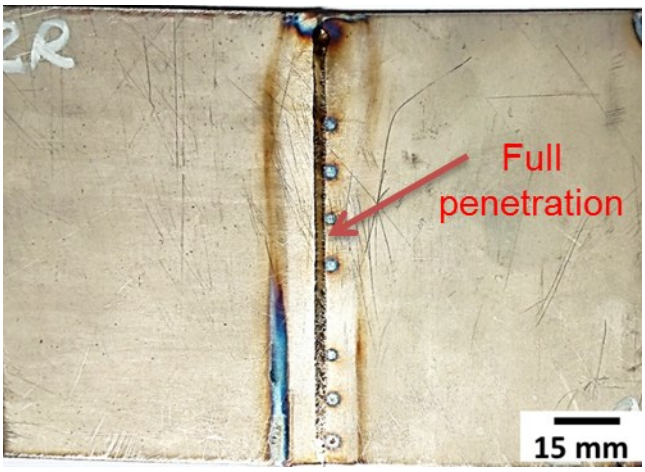

(b)

Top View

Bottom View

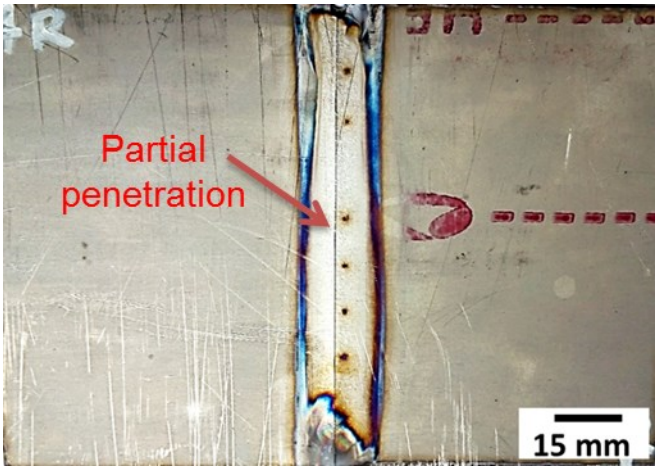

(c)

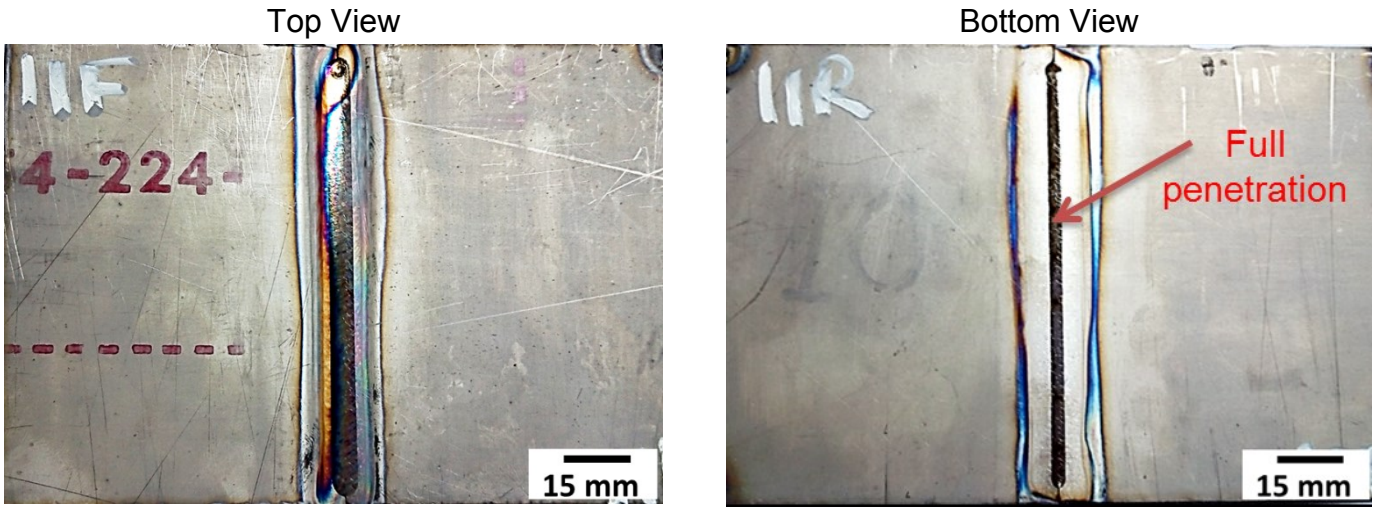

(d)

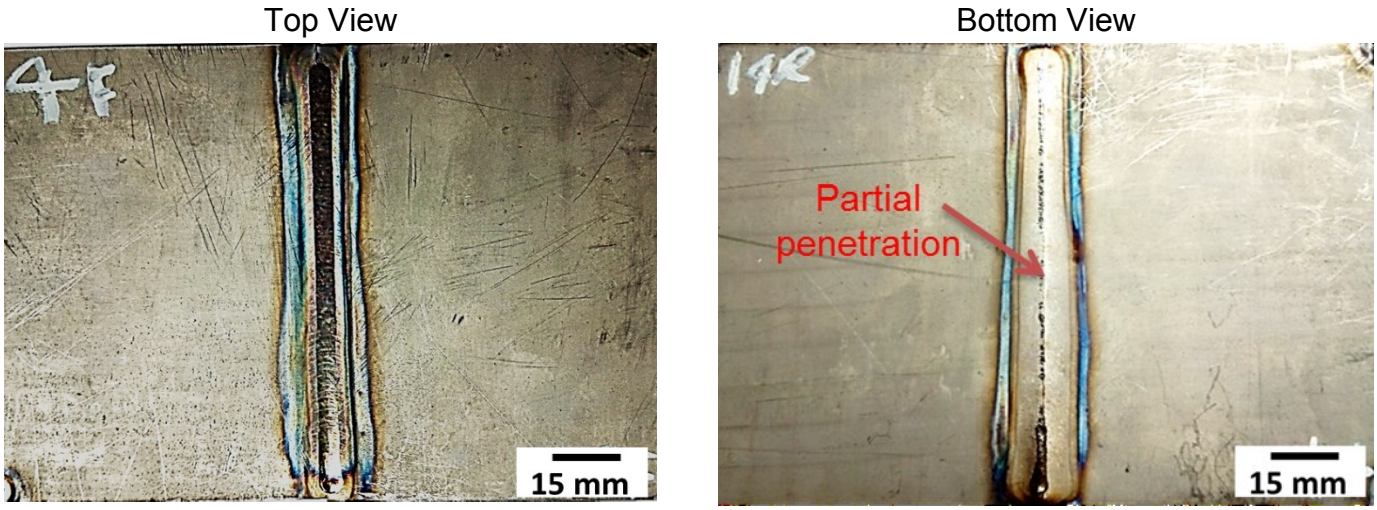

Figure 1. Top and bottom side images of the samples for different welding conditions in Table 5 (a) No. 2, (b) No. 4, (c) No.11, (d) No. 14

Furthermore, the microstructural examination of the cross-sectional profile of the weld zone was also performed. The optical images showing grain size and texture of the BM/HAZ region and FZ for the welding condition of No. 2 and No. 4 are presented in Figure 2 and Figure 3 respectively. The FZ and HAZ regions are marked by the presence of coarse grains as compared to the BM region. Since the weld pool in sample No. 4 has not appeared at the bottom edge of the samplein Figure 1(b), it must be considered as a partial penetration weldment. However, the cross-sectional profile

of the FZ in Figure 3 showed coarse prior β grains throughout the thickness: microstructure significantlydifferent than BM suggesting that FZ extends throughout the thickness. Furthermore, the presence of the coarse prior β grains are also present at the HAZ/FZ boundary, the zone of transition from FZ to HAZ (weld pool boundary) cannot be identified correctly from the micrographs. Hence, the depth of penetration cannot be measured from the cross-sectional profiles of the metallographic specimens and the weldments can only be categorized full or partial penetration weldments (as in **Table 4**) by observing the appearance of molten pool at the bottom side of the samples.

(a) **(b)**

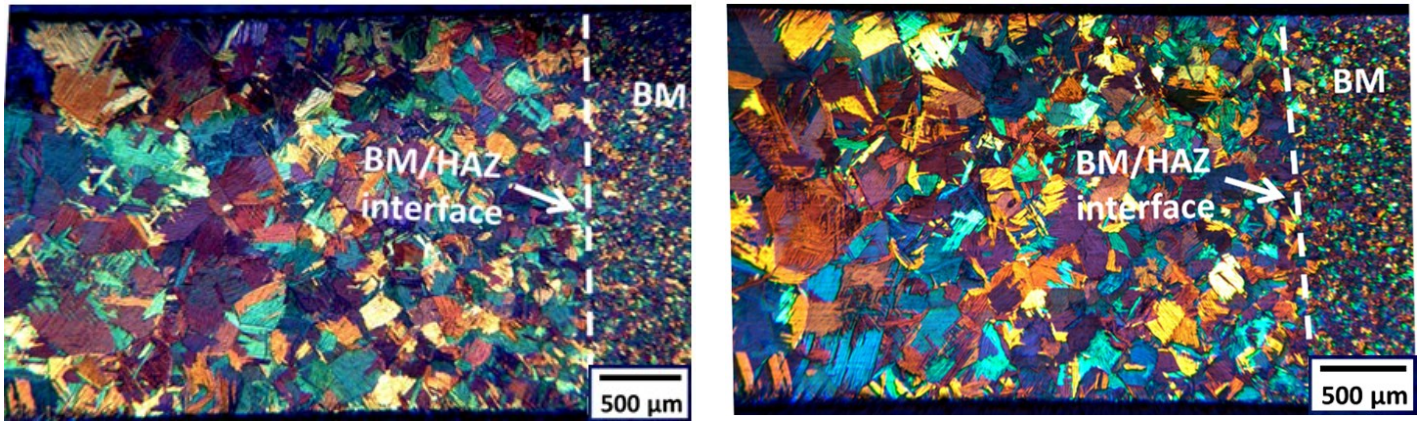

Figure 2. Cross-sections of the HAZ/BM interface for the welding conditions of (a) No. 2 (b) No. 4 in Table 5.

(a) **(b)**

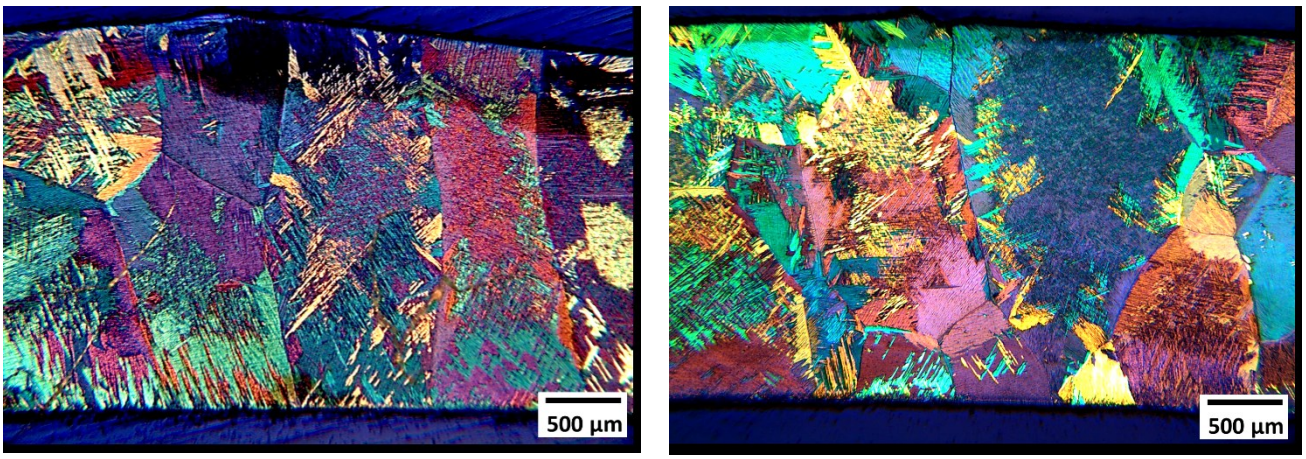

Figure 3. Cross-sections of the FZ for the welding conditions of (a) No. 2 (b) No. 4in Table 5.

Residual stresses

Residual stresses have specific distribution across the width of the welded sample. Initially, three samples were chosen in order to locate the maximum residual stresses in longitudinal and transverse directions. The welded samples with extreme values of welding input parameters (welding speed, peak and background current) were selected for residual stress measurement. Welding parameters for the chosen welding conditions are shown in Table 5. Figure 4 shows the location of strain gauge rosettes installed on the samples.After the measurement of relieved strains, the residual stresses in the longitudinal and transverse direction were used to calculate the Von-Mises stresses. Since Von-Mises stress combines the effect of both longitudinal and transverse residual stresses, its maximum value would indicate the location at which overall values of residual stress are of critical importance. Moreover, the use of Von-Mises criteria for assessment of structural integrity has been reported in available literature [21–25]. Figure 5 shows the Von-Mises residual stress distribution in which it can be seen that the maximum value lies at the location closest to the weld centerline. Hence, for the other 12 welded samples, strain gauge rosettes were only installed at the location closest to the weld bead, which is 3 mm from the weld centerline (Figure 6).

Table 5. Welding parameters for measuring residual stress distribution in the welded samples

Std. Order	Run. Order	Factors		
		Peak current	Back current	Speed
		A	A	mm/min
2	7	36	12	30
3	11	24	18	30
11	5	30	12	36

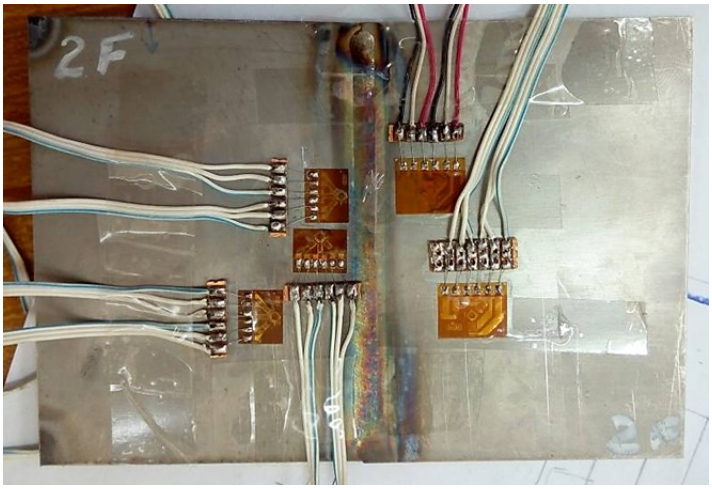

Figure 4. Images showing the strain gauges installed on the welded samples with Std. order No. 2.

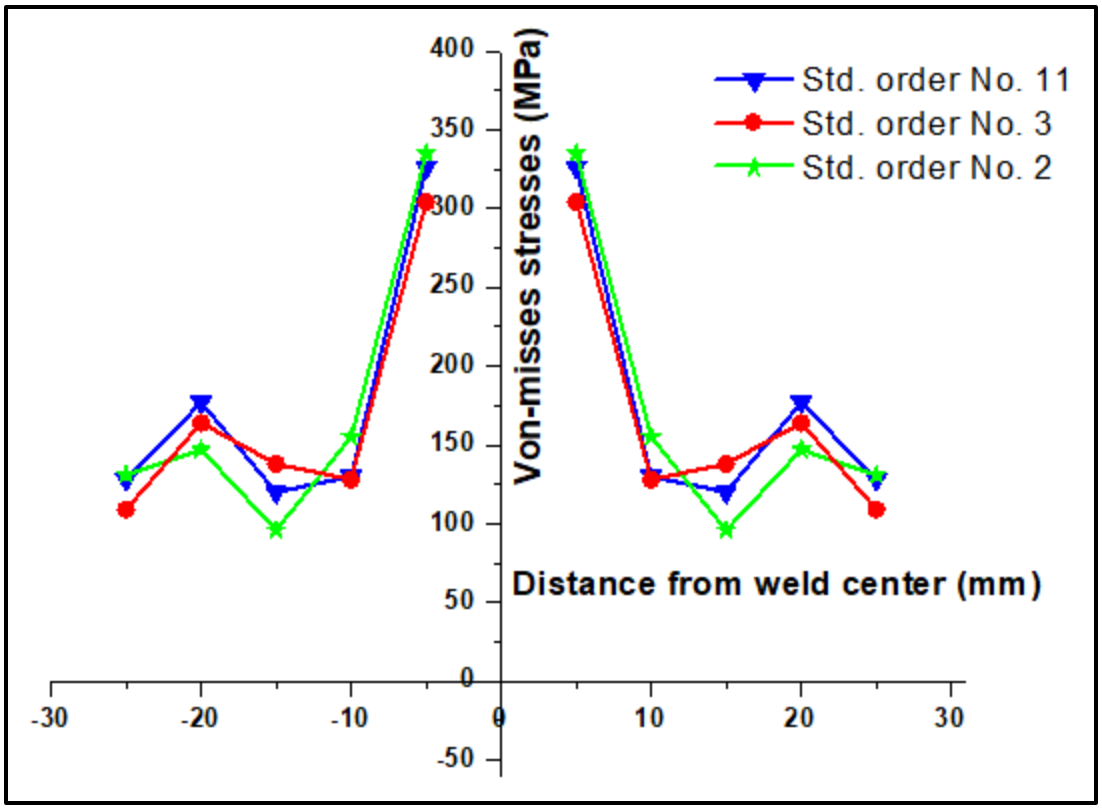

Figure 5. Residual stress (Von-Mises) distribution in the selected welded sampDles

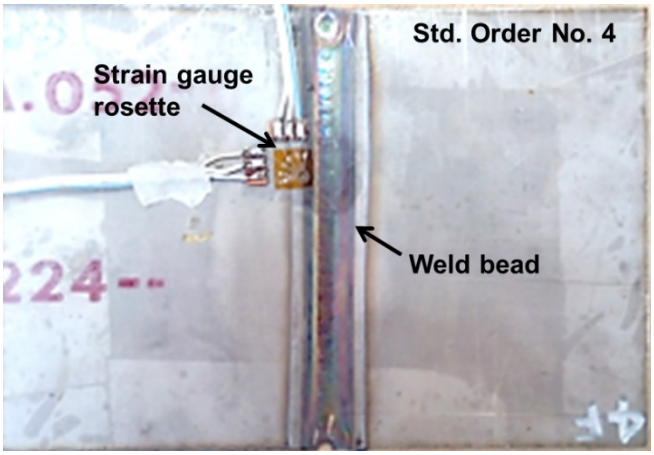

Figure 6. Images showing location of single strain gauge installed on the welded samples with Std. order No. 4.

In order to further study the BBD model, the longitudinal and transverse residual stress values close to the weld centerlinewere considered as given in Table 5. The output fit summary for the response of longitudinal and transverse residual stress is shown in Table 6 and

Table 7. It can be seen that a linear model showed the highest statistical significance for both these responses due to the high value of R-squared and an acceptable p-value for sequential model sum of squares (lower than 0.05 corresponding to a confidence level of 95%).Furthermore, the analysis of variance (ANOVA)in Table 8 showed that only the main effects of R and S are significant for both longitudinal and transverse residual stresses. Figure 7 and Figure 8 show the relationship between actual and predicted values of residual stresses. The mathematical expressions for longitudinal and transverse residual stresses in terms of actual and coded factors are shown by Eq. (1) to Eq. (4).

$$Longitudinal\ residual\ stress = 231.87 + 25.37B - 32.13C \quad (1)$$

$$Longitudinal\ residual\ stress = 255.6 + 8.45R - 5.35S \quad (2)$$

$$Transverse\ residual\ stress = 95.27 + 22.25B - 25.88C \quad (3)$$

$$Transverse\ residual\ stress = 127.76 + 7.41R - 4.31S \quad (4)$$

Table 6. Fit summary for longitudinal residual stress

	Sequential	**Lack of Fit**	**Adjusted**	**Predicted**	**Remarks**
Source	**p-value**	**p-value**	**R-Squared**	**R-Squared**	
Linear	0.0003	0.3255	0.7607	0.6158	Suggested
2FI	0.2531	0.3544	0.7969	0.4594	
Quadratic	0.7947	0.2354	0.7308	-0.3215	
Cubic	0.2354		0.8897		Aliased

Table 7. Fit summary for transverse residual stress

	Sequential	Lack of Fit	Adjusted	Predicted	Remarks
Source	**p-value**	**p-value**	**R-Squared**	**R-Squared**	
Linear	< 0.0001	0.4887	0.9082	0.8568	Suggested
2FI	0.9396	0.3755	0.8797	0.6811	
Quadratic	0.8795	0.2361	0.8298	0.1648	
Cubic	0.2361		0.9301		Aliased

Table 8. ANOVA (analysis of variance) results for longitudinal residual stress

	Sum of		Mean	F	p-value	**Remarks**
Source	**Squares**	**df***	**Square**	**Value**	**Prob> F**	
Model	9382.75	3	3127.58	15.84	0.0003	significant
A-peak current	66.13	1	66.13	0.33	0.5745	
B-back current	3960.50	1	3960.50	20.06	0.0009	
C-Speed	5356.13	1	5356.13	27.12	0.0003	
Residual	2172.18	11	197.47			
Lack of Fit	1990.18	9	221.13	2.43	0.3255	not significant
Pure Error	182.00	2	91.00			

*df: Degree of freedom

Table 9. ANOVA (analysis of variance) results for transverse residual stress

	Sum of		Mean	F	p-value	**Remarks**
Source	**Squares**	**df***	**Square**	**Value**	**Prob> F**	
Model	13439.25	3	4479.75	47.18	< 0.0001	significant
A-peak current	32.00	1	32.00	0.34	0.5733	
B-background current	5151.12	1	5151.12	54.25	< 0.0001	
C-Speed	8256.13	1	8256.13	86.95	< 0.0001	
Residual	1044.48	11	94.95			
Lack of Fit	899.82	9	99.98	1.38	0.4887	not significant
Pure Error	144.67	2	72.33			

*df: Degree of freedom

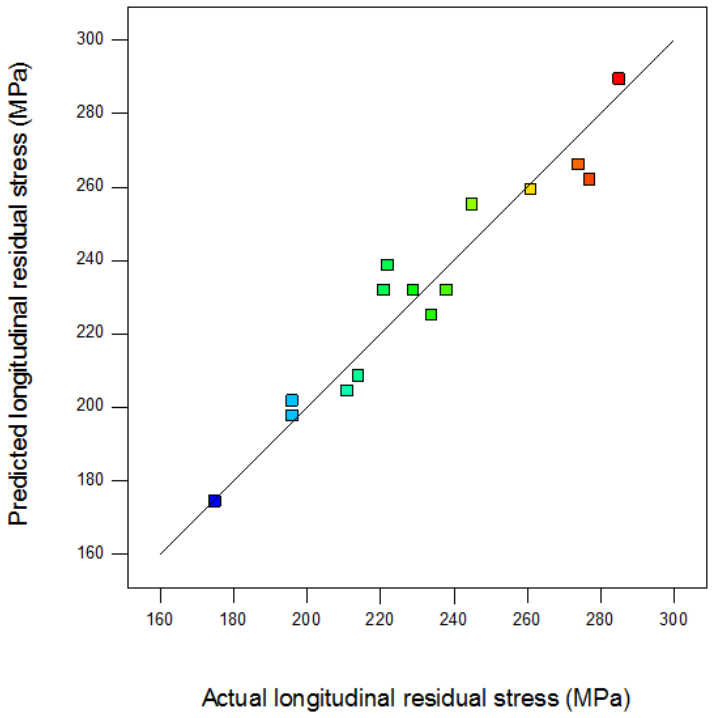

Figure 7. Scatter plot for longitudinal residual stress

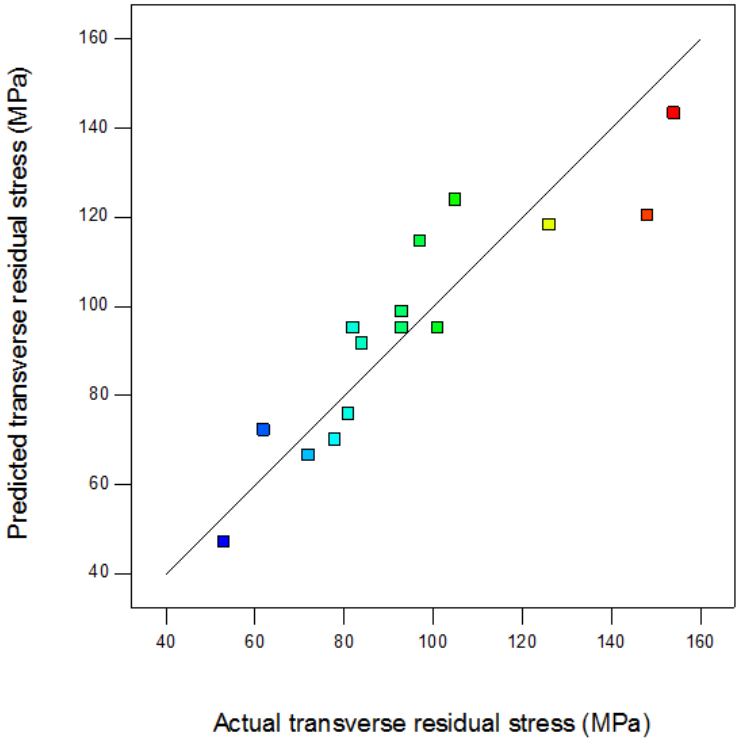

Figure 8. Scatter plot for transverse residual stress

The surface graphs and single factor interaction curves in Figure 9 to Figure 15show the variation in longitudinal and transverse residual stresses at a distance of 3 mm from the weld centerline, due to the change in welding parameters. Figure 9 and Figure 11 show that longitudinal and transverse residual stresses were not considerably influenced due to a change in the peak current, however a significant variation was observed due to a change in the background current. Similarly Figure 10 and Figure 12 show that a significant variation inlongitudinal and transverse residual stresses was observed due to a change in the welding speed. Hence, both longitudinal and transverse residual stresses are a strong function of background current and welding speed.

Higher heat input and reduction in cooling rate favors the generation of thermal strains and hence the overall magnitude of residual stress increases [26]. Olabi et al. (2007) used multiple DOE techniques to study the effect of laser welding parameters on the residual stress in HAZ region of AISI 304 weldments [14]. They also concluded that reduced laser power and high welding speed led to low levels of induced residual stresses. It is also interesting to note that both peak and background current are directly proportional to the heat input, however background current has a main effect on the residual stresses, whereas peak current has a non-significant effect. This may be attributed to the fact that an increase in background current decreases the temperature gradients and cooling rate, whereas increasing the peak current increased heat input. However, the peak temperatures and cooling rates also increases due to an increase of peak current. An increased cooling rate also favors the α' martensite formation which according to Appolaire et al. (2015), produced a compressive volumetric strains and opposed the induced tensile thermal strains as a result of increased heat input [27].

The generation of compressive volumetric and tensile thermal stresses are due to increase in peak current and these stresses tend to balance each other, eventually resulting in no change in overall residual stresses due to variation in peak current. In some cases, the compressive stresses generated due to volumetric change may be slightly more than the thermal stresses. This may lead to a marginal increase in

magnitude of the overall residual stresses, with the increase in peak current.Furthermore, welding speed was found to have the most dominant influence on the longitudinal and transverse residual stresses. Increasing the welding speed reduced the effective time required by the heat source for melting which further increased the cooling rate and a reduced residual stresses were observed.

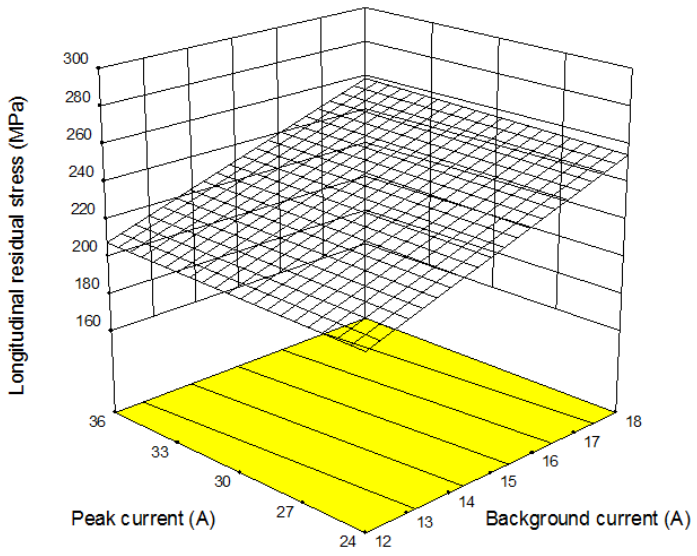

Figure 9. Effect of peak and background current on longitudinal residual stress at a welding speed of 30 mm/min

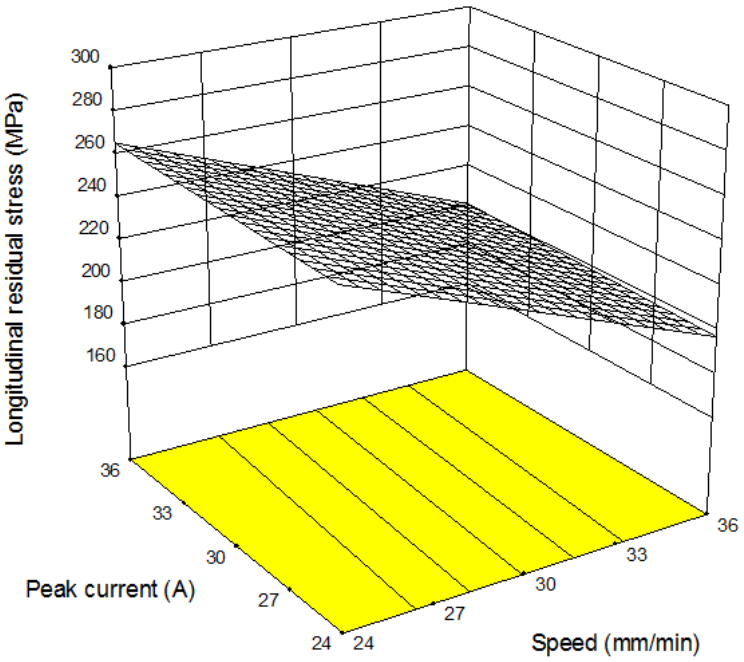

Figure 10. Effect of peak current and speed on longitudinal residual stress at a background current of 15 A

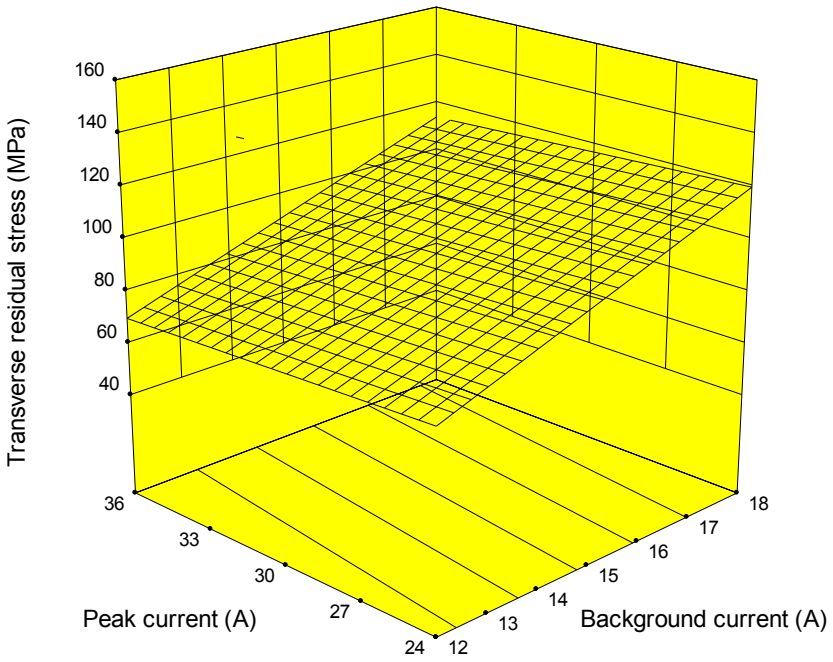

Figure 11. Effect of peak and background current on transverse residual stress at a welding speed of 30 mm/min

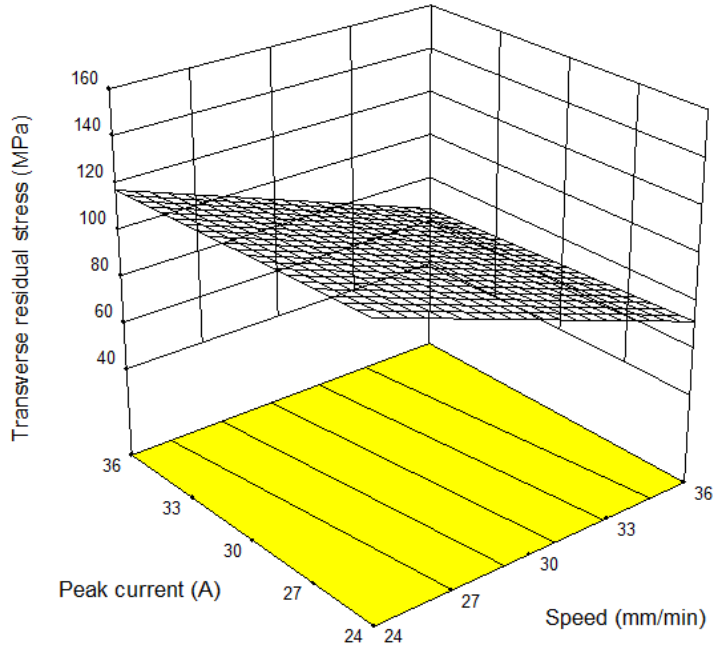

Figure 12. Effect of peak current and speed on transverse residual stress at a background current of 15 A

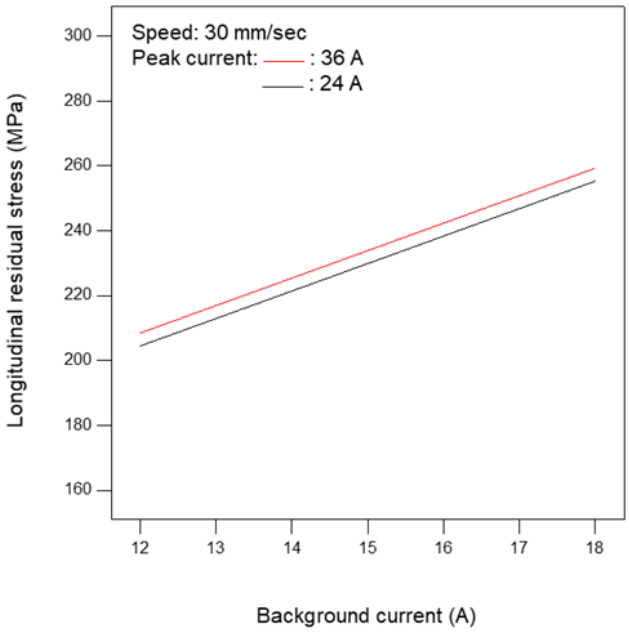

Figure 13. Effect of background current on longitudinal residual stress

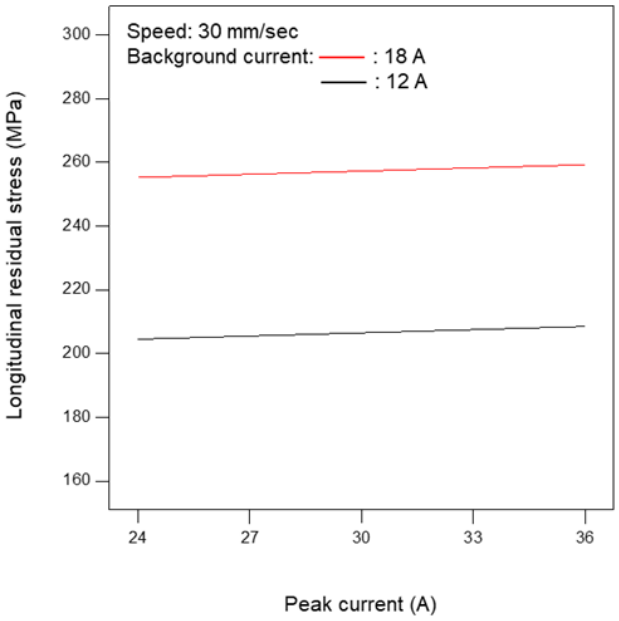

Figure 14. Effect of peak current on longitudinal residual stress

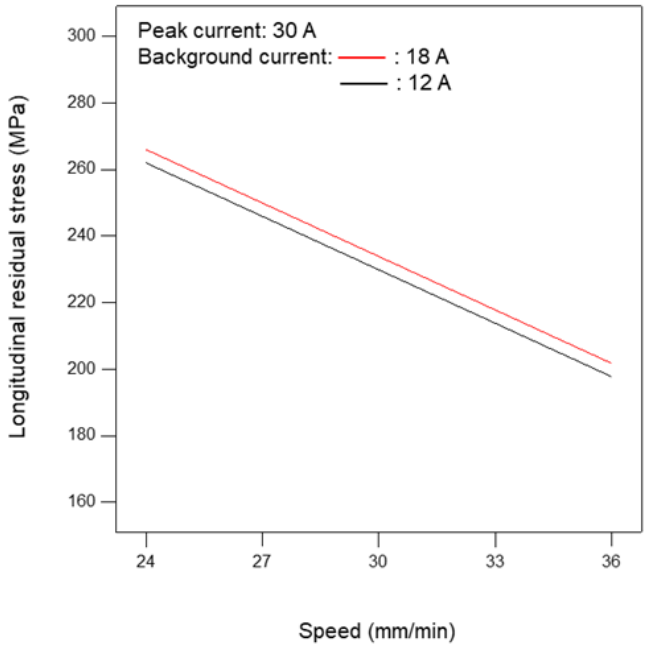

Figure 15. Effect of welding speed on longitudinal residual stress

Optimization of residual stresses

Table 10 presents a summary of the three different criteria which were chosen for the multi-response optimization of the P-TIG welding process. The first criterion focused on the residual stresses only and the objective was to minimize the residual stresses without any constraints on the other output responses. In the second criteria, a more practical approach was used. Constraints were applied on the joint penetration and residual stresses. In terms of quality, the weld joints are examined through radiographic testing (RT) in which partial penetration joints were not acceptable and only full penetration joints qualified the radiographic examination. In full penetration weldments, the molten weld pool appeared at the bottom side of the samples, hence completely filling the gap between the two samples in the butt joint. In partial penetration butt weldments, the unfilled gap between the two samples acts as a zone of stress concentration during the cyclic loading and may cause premature crack initiation [28,29]. To avoid this situation the goal for the response of penetration was to target a value of "1", which corresponded to full penetration butt weldments. Moreover, the goal was to minimize the longitudinal and transverse residual stresses. The desirability function was further improved by setting an importance level of "5" to the response of penetration and a level of "3" for residual stresses. In this approach, an importance level of "5" means that the optimization algorithm in Design-Expert V7 will first look for those points in the design space which corresponded to full penetration weldments and then apply rest of the constraints included in the optimization criterion.

Table 10. Description of detailed criteria for optimization of the P-TIG welding process

Factors and responses	Range		Criteria	
	Lower	Upper	First	Second
Peak current (A)	24	36	In range	In range
Background current (A)	12	18	In range	In range
Welding speed (mm/min)	24	36	In range	In range
Penetration (0,1) 0=partial, 1=full	0	1	None	Equal to 1 (Ord. of importance =5)
Longitudinal residual stress (MPa)	175	285	Minimize (Ord. of importance =3)	Minimize (Ord. of importance =3)
Transverse residual stress (Mpa)	53	154	Minimize (Ord. of importance =3)	Minimize (Ord. of importance =3)

Table 11 presents the optimized welding conditions required to achieve maximum desirability in the different optimization criteria. It can be further observed that in order to satisfy the first criterion (minimizing the residual stresses) the peak current could vary in the range 24.0 A to 24.2 A, background current from 12.0 A to 12.1 A and welding speed from 35.8 mm/min to 36 mm/min. Since there was insignificant variation in the ranges of the welding input factors for satisfying second criterion so a peak current of 24 A, background current of 12 A and welding speed of 36 mm/min was chosen. This corresponded to the first solution of the first criterion with a desirability of 0.8 as shown in Table 11 and the graphical form of this optimal solution is presented in Figure 16. The longitudinal and transverse residual stresses increased as the heat input increased in P-TIG welding process which was directly related to peak current and background current and inversely related to welding speed. Hence the first criterion was satisfied when a high welding speed and lowest values of the peak and background current were chosen.

Table 11. Solution set for the optimized welding conditions based on the different criteria

Input factors			Output responses			
Peak current (A)	Background current(A)	Welding Speed (mm/min)	Penetration (full=1. Partial =0)	Longitudinal residual stress (MPa)	Transverse residual stresses (MPa)	Desirability
24.0	12.0	36.0	0	172.4	50.0	0.8
36.0	16.70	36.0	1	216.1	79.1	0.824

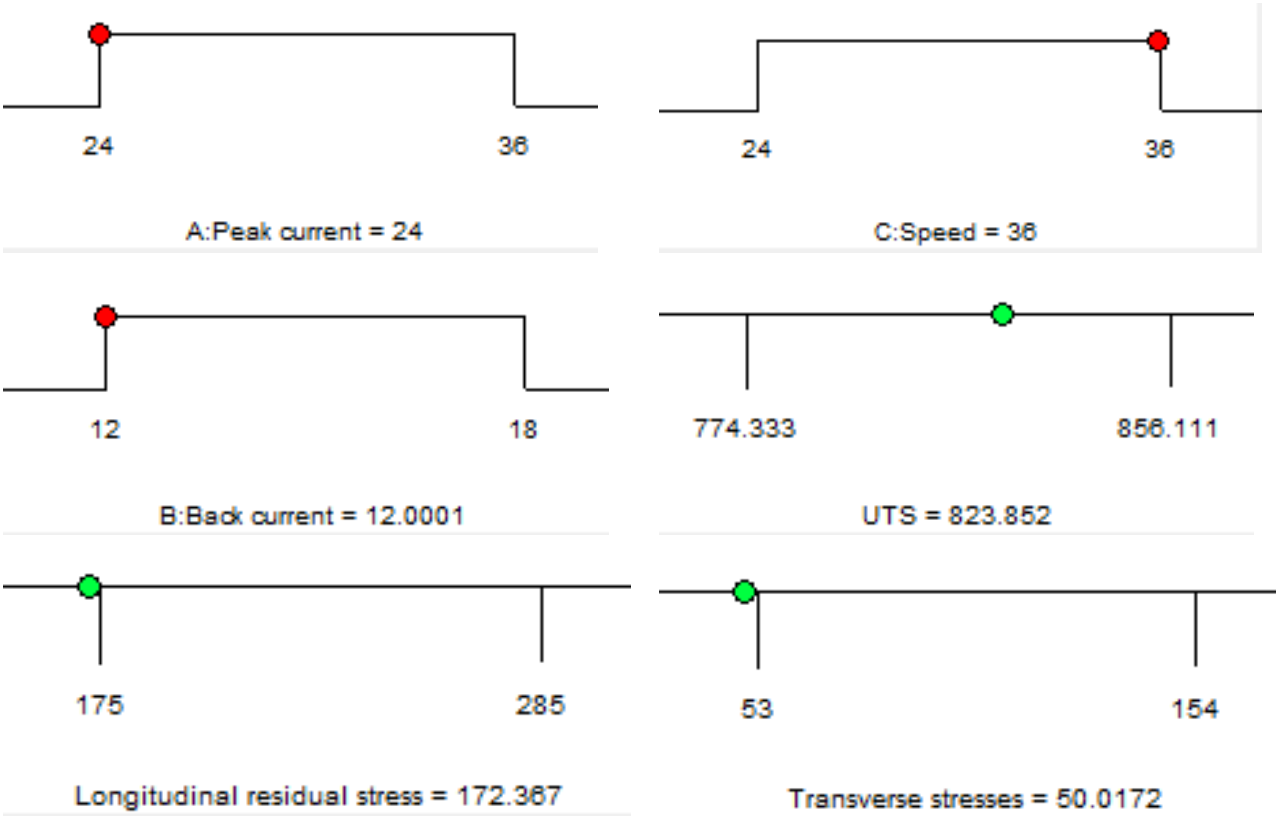

Figure 16. Graphical representation of the optimal solution based on first criterion

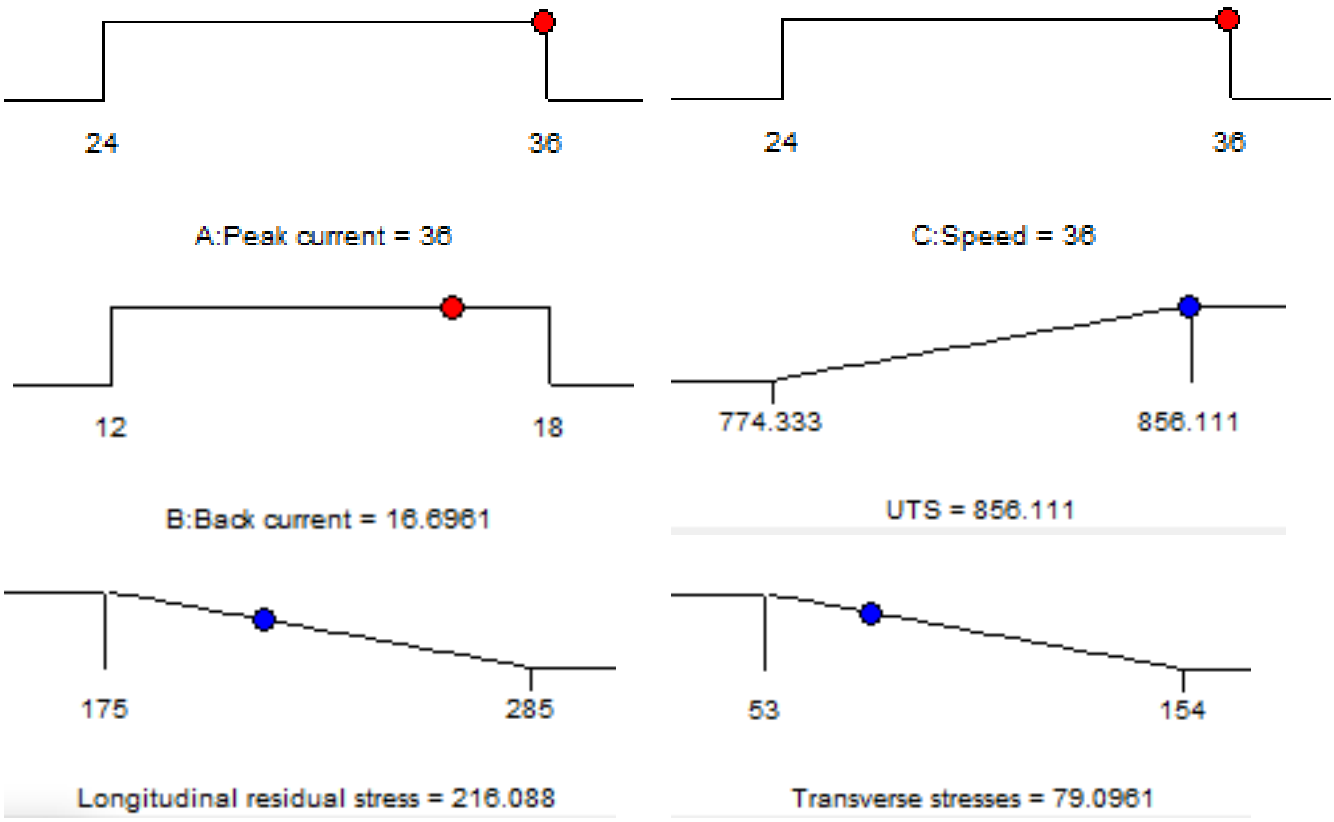

Figure 17. Graphical representation of the optimal solution based on second criterion

To optimize the welding process according to second criteria (full penetration, minimum residual stresses), Table 11 shows that peak current and welding speed should be 36 A and 36 mm/min respectively whereas, background current should be in the range 16.57 A to 16.93 A. It should be noted that in order to achieve full penetration, heat input should be significant enough to extend the weld pool up to the bottom surface. This phenomenon is favored at a high value of peak and background current and a low value of welding speed. However, since the second criterion is established for multi response optimization, the overall desirability will not be maximized since longitudinal and transverse residual stresses tend to increase at low welding speed and high background current. Moreover, it can also be observed that a maximum desirability of 0.824 is achieved which is less than unity. This is due to the fact that in order to achieve full penetration, background current has to be increased so that enough heat is available for the weld pool to reach full depth. At the same time, more residual stresses

are generated due to increased heat input. Hence, the two goals cannot be fully achieved at the same time and the best possible solution set satisfying all the goals is as proposed in Table 11. From this set, the 1st solution was chosen which resulted in minimum value of residual stresses as compared to other solutions. This is also shown in graphical form in Figure 17.

Figure 18 and Figure 19 presents the overlay graph using which the optimal region based on the first and second criterion can be presented graphically. The colored/shaded area in the plot represents the region where the optimal conditions can be achieved. These overlay plots are particularly important for technical use while practically performing the welding operation. Using these graphs, the welding operator can choose a combination of welding input parameters to attain the desirable response values.

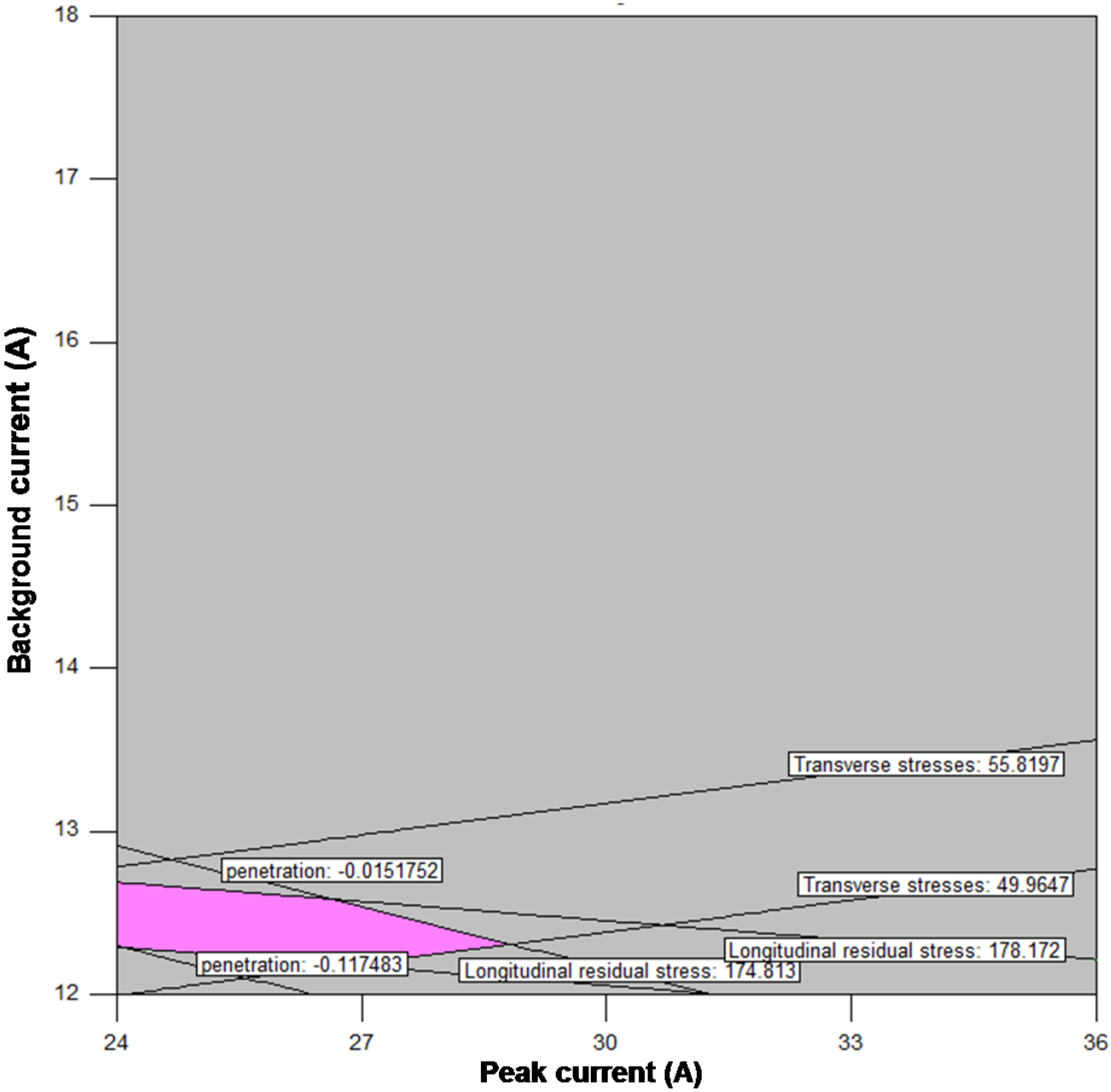

Figure 18. Overlay plots showing the feasible region (pink) of the optimal welding conditions to satisfy the first criterion.

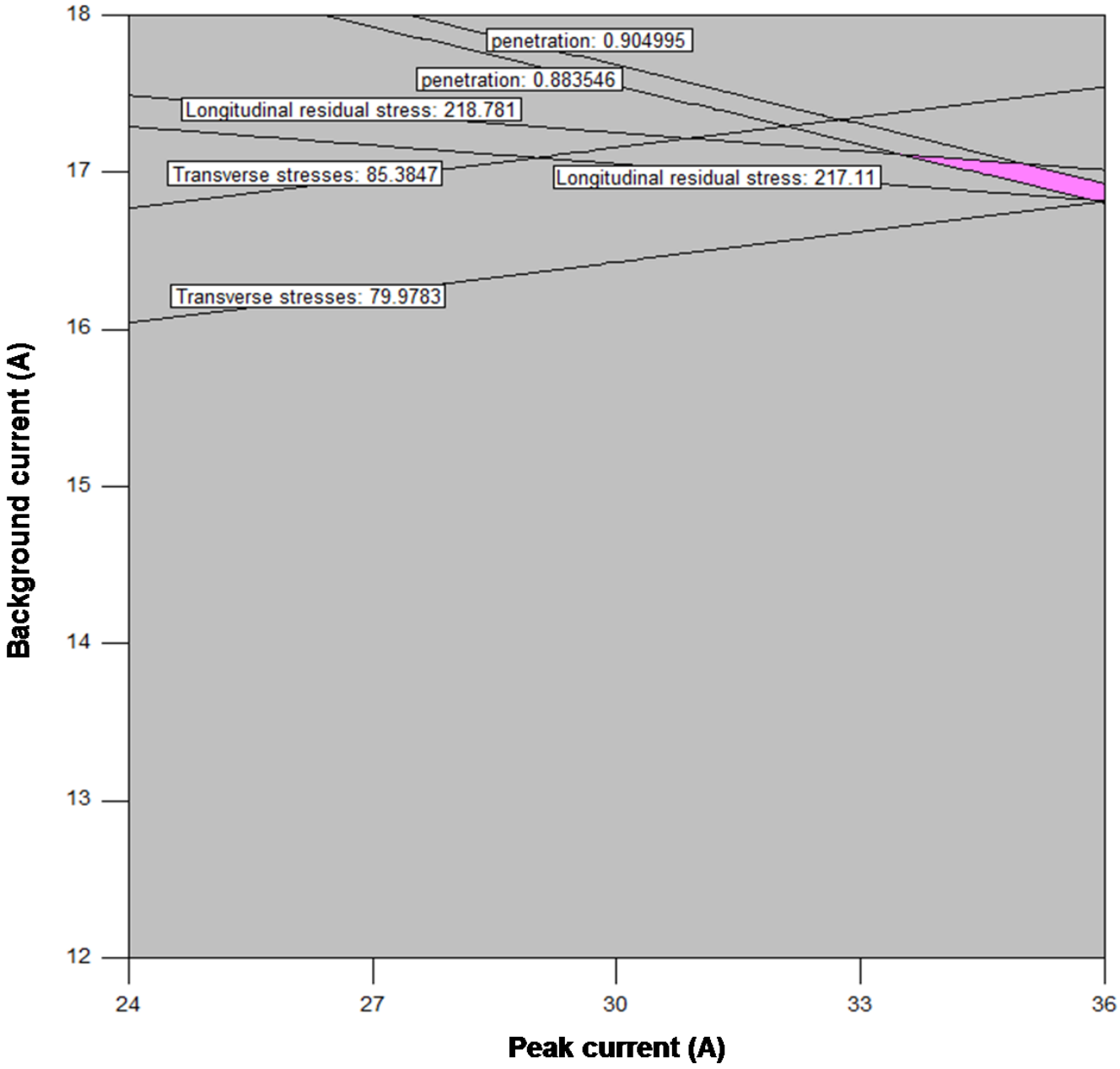

Figure 19. Overlay plots showing the feasible region(pink) of the optimal welding conditions to satisfy the second criterion.

Validation of the developed models

Validation experiments were performed to measure the weld pool characteristics, residual stresses, tensile and impact properties of the optimal weldments and the results are shown in Table 12. The residual stresses were measured close to the weld

centerline only in the optimal weldment of the first criterion as shown in Figure 20. For the optimal weldment of second criterion, a complete residual stress distribution was measured (Figure 20). In the author's previous work, the influence of TIG, LBW and EBW on the microstructure, mechanical properties and residual stresses in full penetration Ti-5Al-2.5Sn alloy weldments was studied. In Figure 21 and Figure 22, the longitudinal and transverse residual stress distribution in the optimal weldment of second criterion was compared with full penetration P-LBW and EBW weldments from the author's previous work[12,30]. It can be seen that close to the weld centerline, longitudinal residual stress magnitude in P-TIG weldments is approx. 222 MPa which is 16% higher than those in EBW weldments. In the transverse direction, residual stress of approx. magnitude 91 MPa, close to the weld centerline are present which are 44% less than those in EBW weldments. This showed that optimal welding conditions in full penetration P-TIG weldments can produce a residual stress distribution comparable to EBW weldments. However, residual stresses in P-LBW are still significantly less than the P-TIG and EBW weldments (longitudinal residual stresses of -27 MPa in P-LBW as compared to 191 MPa in EBW and 222 in P-TIG weldments close to the weld centerline).

Table 12. Validation of the optimized welding conditions through experiments

Criterion number	Input factors				Output responses		
	Peak current (A)	Background current(A)	Welding Speed (mm/min)		Penetration (full=1. Partial =0)	Longitudinal residual stress (MPa)	Transverse residual stresses (MPa)
1	24	12	36	**Predicted**	0	172.4	50.0
				Actual	0	152.5	48.8

				%Error	0	11.5	2.4
2	36	17	36	**Predicted**	1	216.1	79.1
				Actual	1	235.8	84.0
				%Error	0	9.1	6.2

(a) **(b)**

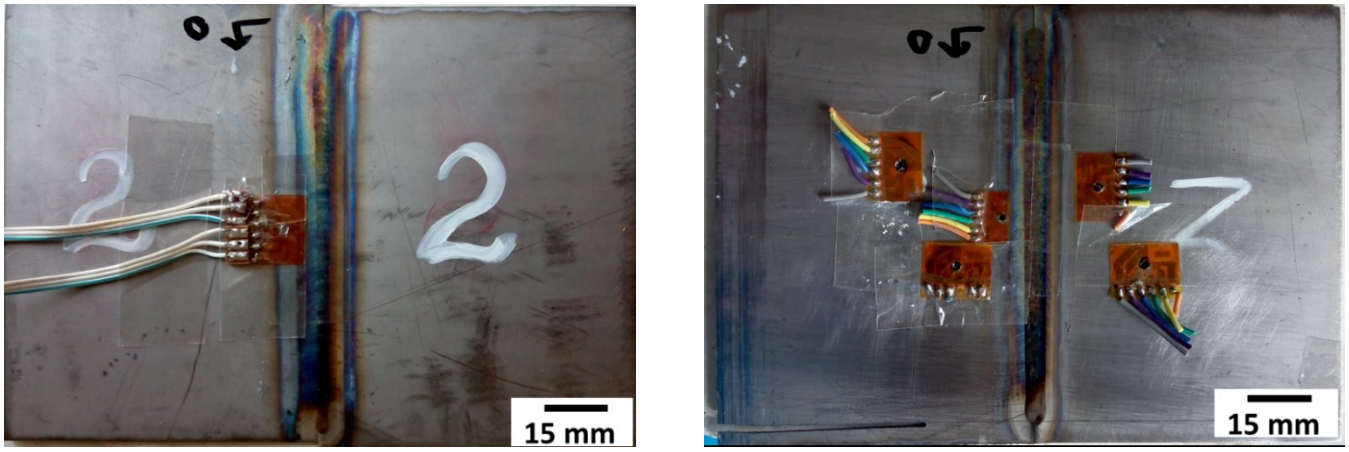

Figure 20. Image showing location of residual stress measurement in the optimal weldments of (a) first criterion and (b) second criterion.

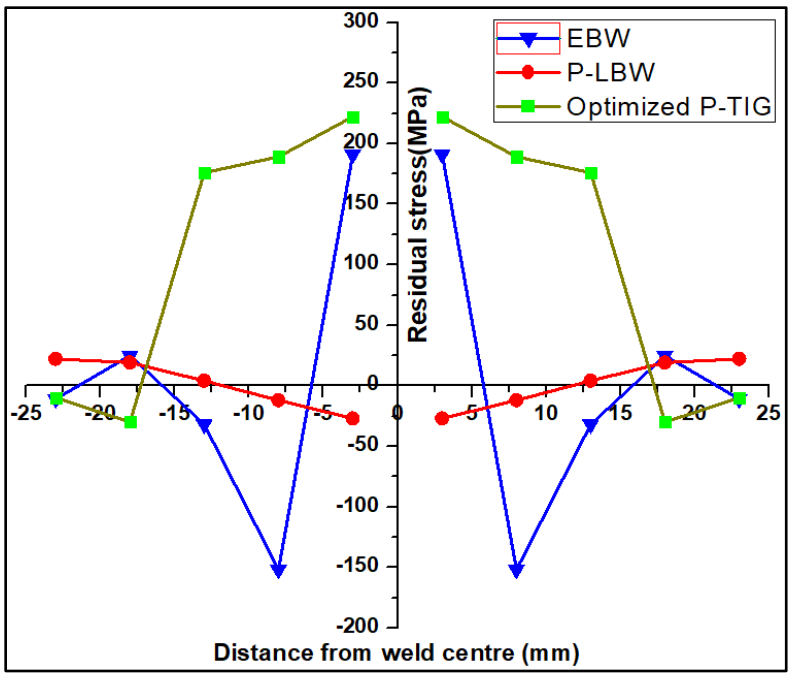

Figure 21. Comparison of longitudinal residual stresses in optimal P-TIG weldments of second criterion with P-LBW and EBW weldments from ref [12,30].

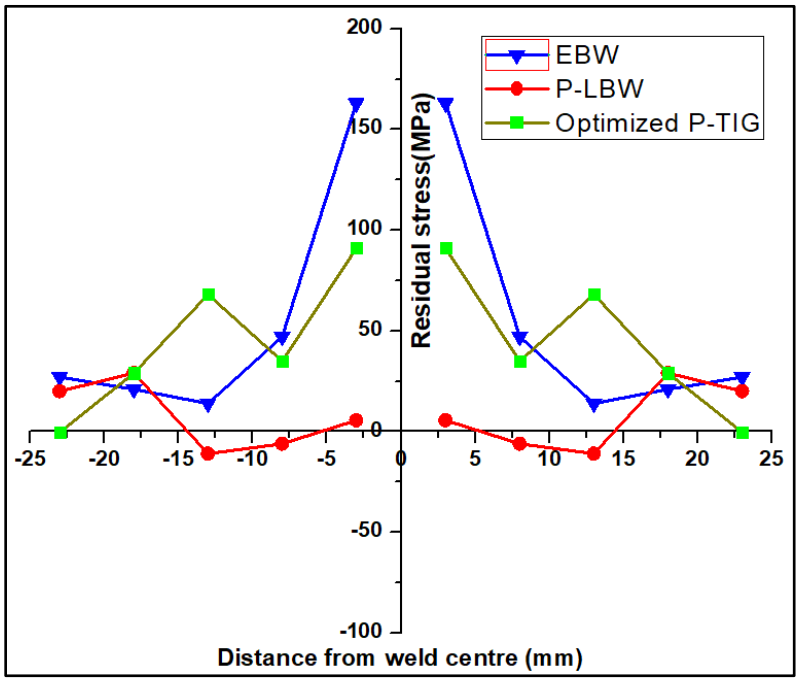

Figure 22. Comparison of transverse residual stresses in optimal P-TIG weldments of second criterion with P-LBW and EBW weldments from ref [12,30].

Conclusions:

The present work aims at improving the pulsed TIG welding process for Ti-5Al-2.5Sn alloy by optimizing both the pulsed current parameters and welding speed in order to achieve minimum residual stresses and complete weld pool penetration. Studies available in literature are focused more on maximizing the joint strength by optimizing the pulsed current only. The suggested criteria provides a solution for a problem usually faced in the welding of titanium alloy sheets. The following conclusions are obtained:

1. Welding speed was found to have the highest influence on the induced residual stresses and a high welding speed was recommended to minimize the residual stresses. This was attributed to a reduction in overall time required for the joining operation when welding is performed at high speed.
2. Reducing the value of background current also favored a reduction in residual stresses by reducing the heat input during the welding process. A minimum value of152 MPa for longitudinal and 49 MPa for transverse residual stress can be attained at welding conditions; peak current of 24 A, background current of 12 A and welding speed of 36 mm/min. However, this also led to partial penetration in the weldments which is considered asof reduced quality and may lead toa reduction in service life of the weldments.
3. An optimization criterion was proposed inwhich the residual stresses were minimized while maintaining full penetration in the weldments. The results showed that for a full penetration weldment, a minimum value of 235 MPa for longitudinal and 84 MPa for transverse residual stress will be attained at welding conditions; peak current of 36A, background current of 17 A and welding speed of 36 mm/min.
4. With the optimum welding parameters in TIG welding, the residual stresses can be reduced significantly and the resultant weld quality can be achieved comparable to the LBW and EBW weldments.

Acknowledgments

The authors would like to thank Ghulam Ishaq Khan Institute ofEngineering Sciences and Technology for providing funding for this project.

Data availability

The processed data required to reproduce these findings cannot be shared at this time as the data also forms part of an ongoing study.

References

1. Montingelli ME, Benyounis KY, Quilty B, et al. Optimisation of biogas production from the macroalgae Laminaria sp. at different periods of harvesting in Ireland. *Appl Energy* 2016; 177: 671–682.
2. Ruggiero A, Tricarico L, Olabi AG, et al. Weld-bead profile and costs optimisation of the CO2 dissimilar laser welding process of low carbon steel and austenitic steel AISI316. *Opt Laser Technol* 2011; 43: 82–90.
3. Ekpeni LEN, Benyounis KY, Stokes J, et al. Improving and optimizing protein concentration yield from homogenized baker's yeast at different ratios of buffer solution. *Int J Hydrogen Energy* 2015; 41: 16415–16427.
4. Eltawahni HA, Olabi AG, Benyounis KY. Investigating the CO2 laser cutting parameters of MDF wood composite material. *Opt Laser Technol* 2011; 43: 648–659.
5. Benyounis KY, Olabi a. G. Optimization of different welding processes using statistical and numerical approaches - A reference guide. *Adv Eng Softw* 2008; 39: 483–496.
6. Olabi AG, Alsinani FO, Alabdulkarim AA, et al. Optimizing the CO2 laser welding process for dissimilar materials. *Opt Lasers Eng* 2013; 51: 832–839.
7. Balasubramanian M, Jayabalan V, Balasubramanian V. Response surface approach to optimize the pulsed current gas tungsten arc welding parameters of Ti−6Al−4V titanium alloy. *Met Mater Int* 2007; 13: 335–344.
8. Balasubramanian M, Jayabalan V, Balasubramanian V. Prediction and optimization of pulsed current gas tungsten arc welding process parameters to obtain sound weld pool geometry in titanium alloy using lexicographic method. *J Mater Eng Perform* 2009; 18: 871–877.
9. Balasubramanian M, Jayabalan V, Balasubramanian V. Effect of microstructure on impact toughness of pulsed current GTA welded α–β titanium alloy. *Mater Lett* 2008; 62: 1102–1106.
10. Balasubramanian M. Developing mathematical models to predict tensile properties of pulsed current gas tungsten arc welded Ti – 6Al – 4V alloy. *Mater*

Des 2008; 29: 92–97.

11. Short AB. Gas tungsten arc welding of α + β titanium alloys: a review. *Mater Sci Technol* 2009; 25: 309–324.
12. Junaid M, Khan FN, Baksh N, et al. Study of microstructure, mechanical properties and residual stresses in full penetration electron beam welded Ti-5Al-2.5Sn alloy sheet. *Mater Des* 2018; 139: 198–211.
13. Junaid M, Rahman K, Khan FN, et al. Comparison of microstructure, mechanical properties, and residual stresses in tungsten inert gas, laser, and electron beam welding of Ti–5Al–2.5Sn titanium alloy. *Proc Inst Mech Eng Part L J Mater Des Appl* 2017; 0: 146442071774834.
14. Olabi AG, Casalino G, Benyounis KY, et al. Minimisation of the residual stress in the heat affected zone by means of numerical methods. *Mater Des* 2007; 28: 2295–2302.
15. Junaid M, Baig MN, Shamir M, et al. A comparative study of pulsed laser and pulsed TIG welding of Ti-5Al-2 . 5Sn titanium alloy sheet. *J Mater Process Technol* 2017; 242: 24–38.
16. Senthil Kumar T, Balasubramanian V, Sanavullah MY. Influences of pulsed current tungsten inert gas welding parameters on the tensile properties of AA 6061 aluminium alloy. *Mater Des* 2007; 28: 2080–2092.
17. Mehdi B, Badji R, Ji V, et al. Microstructure and residual stresses in Ti-6Al-4V alloy pulsed and unpulsed TIG welds. *J Mater Process Technol* 2016; 231: 441–448.
18. Tchoumi T, Peyraut F, Bolot R. Influence of the welding speed on the distortion of thin stainless steel plates - Numerical and experimental investigations in the framework of the food industry machines. *J Mater Process Technol* 2016; 229: 216–229.
19. Subravel V, Padmanaban G, Balasubramanian V. Effect of welding speed on microstructural characteristics and tensile properties of GTA welded AZ31B magnesium alloy. *Trans Nonferrous Met Soc China (English Ed* 2014; 24: 2776–2784.
20. Benyounis KY, Olabi AG, Hashmi MSJ. Multi-response optimization of CO2 laser-welding process of austenitic stainless steel. *Opt Laser Technol* 2008; 40: 76–87.
21. Adamus K, Kucharczyk Z, Wojsyk K, et al. Numerical analysis of electron beam welding of different grade titanium. *Comput Mater Sci* 2013; 77: 286–294.
22. Kohandehghan a. R, Serajzadeh S, Kokabi a. H. A Study on Residual Stresses in Gas Tungsten Arc Welding of AA5251. *Mater Manuf Process* 2010; 25: 1242–1250.
23. Nasim K, Arif a. FM, Al-Nassar YN, et al. Investigation of residual stress development in spiral welded pipe. *J Mater Process Technol* 2015; 215: 225–238.
24. Rahman Chukkan J, Vasudevan M, Muthukumaran S, et al. Simulation of laser butt welding of AISI 316L stainless steel sheet using various heat sources and

experimental validation. *J Mater Process Technol* 2015; 219: 48–59.

25. Paulo RMF, Carlone P, Valente R a. F, et al. Influence of friction stir welding effects on the compressive strength of aluminium alloy thin-walled structures. *Key Eng Mater* 2014; 611–612: 184–190.
26. Murakawa H. 13 - Residual stress and distortion in laser welding. *Woodhead Publ Ser Electron Opt Mater* 2013; 2: 374–400e.
27. Appolaire B, Settefrati A., Aeby-Gautier E. Stress and strain fields associated with the formation of α" in near-β titanium alloys. *Mater Today Proc* 2015; 2: S589–S592.
28. Ferro P, Berto F, James MN. Asymptotic residual stresses in butt-welded joints under fatigue loading. *Theor Appl Fract Mech* 2016; 83: 114–124.
29. Wang SQ, Li WY, Zhou Y, et al. Tensile and fatigue behavior of electron beam welded dissimilar joints of Ti – 6Al – 4V and IMI834 titanium alloys. 2016; 649: 146–152.
30. Junaid M, Khan FN, Rahman K, et al. Effect of laser welding process on the microstructure, mechanical properties and residual stresses in Ti-5Al-2.5Sn alloy. *Opt Laser Technol* 2017; 97: 405–419.